

ARTICLE OPEN



YTHDF1/SLC39A4 signaling axis promotes gastric cancer cell proliferation by suppressing cuproptosis ex vivo and in vitro

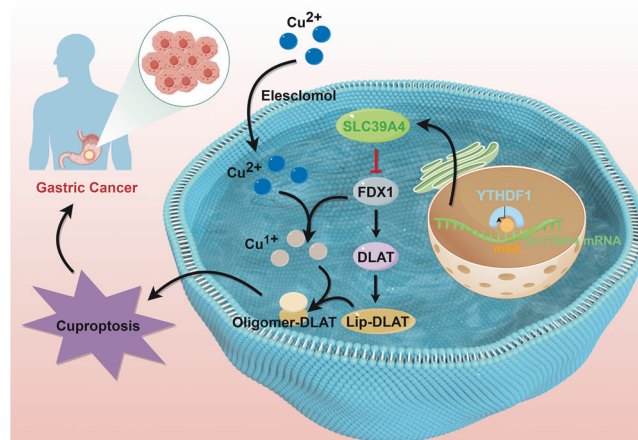
Jingying Su^{1,2,3}, Jihan Qi^{1,3}, Binhua Xu², Jiaxin Wang¹, Ram Prasad Chaulagain¹, Hongliang Chen¹, Ning Li¹, Xinyu Jiang¹, Lingyi Xu¹, Fengchun Li¹, Wenli Mao¹ and Shizhu Jin¹

© The Author(s) 2026

Gastric cancer (GC) continues to be a major contributor to global cancer mortality, underscoring the need to elucidate its molecular mechanisms to develop effective therapies. Cuproptosis, a copper-dependent form of cell death, exhibits tumor-suppressive effects in GC. Clinical specimens revealed elevated expression of solute carrier family 39 member 4 (SLC39A4) in GC tissues, correlating with poor prognosis. However, the role of SLC39A4 in GC remains unclear. Using lentiviral transduction in AGS and MKN-45 cell lines, we established stable monoclonal strains with SLC39A4 overexpression and knockdown for functional studies. SLC39A4 promotes GC cell proliferation both in vitro and in vivo. CuCl₂ and elesclomol treatment induced cuproptosis, which was attenuated by SLC39A4 overexpression but potentiated by SLC39A4 knockdown, as confirmed through proliferation assays and cuproptosis marker analyses in cell cultures and xenograft models. Mechanistically, the m6A reader protein YTHDF1, frequently overexpressed in GC patients and known to inhibit elesclomol-induced cuproptosis, bound to SLC39A4 mRNA and stabilized its transcripts. Dual-luciferase assays demonstrated that mutation of the m6A site within SLC39A4's coding sequence abolished YTHDF1-mediated regulation. These findings establish SLC39A4 as a promoter of GC progression through cuproptosis suppression, modulated by YTHDF1 via m6A-dependent mRNA stabilization, revealing potential therapeutic targets for GC treatment.

Cancer Gene Therapy; <https://doi.org/10.1038/s41417-026-01036-5>

Graphical Abstract



INTRODUCTION

Gastric cancer (GC) is a common malignant tumors [1], with over one million new cases diagnosed each year [2]. The mortality rate of GC ranks fifth among all malignant tumors [3]. Although advances in medical technology have improved patient prognosis to some extent, the overall outlook remains unsatisfactory

because most patients are diagnosed at an advanced stage [4]. Exploring new therapeutic strategies and understanding the pathogenesis of GC are crucial for improving patient prognosis.

Cuproptosis is a recently identified form of copper-dependent cell death, distinct from all other known regulated cell death pathways [5]. Excess intracellular Cu²⁺ can be transported to the

¹Department of Gastroenterology and Hepatology, the Second Affiliated Hospital of Harbin Medical University, Harbin, China. ²Department of Endocrinology, Harbin the First Hospital, Harbin, China. ³These authors contributed equally: Jingying Su, Jihan Qi. email: drshizhujin@hrbmu.edu.cn

Received: 18 August 2025 Revised: 9 March 2026 Accepted: 16 April 2026

Published online: 29 April 2026

mitochondria via ionophores and reduced to cuprous ion (Cu^{1+}). This process induces cell death by binding to the lipid components from the tricarboxylic acid cycle, promoting aggregation of lipoylated proteins and loss of iron-sulfur cluster proteins [6]. Targeting the promotion of cuproptosis has been reported as a promising strategy to inhibit GC [7].

Cuproptosis-related genes (CRGs) regulate the progression of various cancers, including GC [8]. Solute carrier (SLC) family 39 member 4 (*SLC39A4*, *ZIP4*), a member of the *SLC39* family, encodes membrane transporters involved in ion transport [9]. Downregulation of *SLC39A4* can reduce the malignant behavior of tumor cells, including hepatocellular carcinoma [10], oral squamous cell carcinoma [11], and pancreatic cancer [12]. However, the role of *SLC39A4* in GC has not yet been determined. Previous studies have found that GC patients with short overall survival often exhibit high expression of *SLC39A4* [13]. Single-cell RNA sequencing analysis of tissues from intrahepatic cholangiocarcinoma revealed that silencing of *SLC39A4* upregulated the level of the cuproptosis-inducing protein ferredoxin 1 (FDX1) [14]. The evidence above suggests a potential role for *SLC39A4* as a CRG. In addition, previous studies have indicated that *SLC39A4* mediates the activation of multiple signaling pathways by regulating the phosphorylation of target proteins [15–18]. However, the detailed molecular mechanism by which *SLC39A4* regulates phosphorylation remains unclear. Based on this, the study investigated the molecular mechanisms underlying the signal cascade mediated by *SLC39A4* using phosphorylation proteomics analysis.

YTH N6-methyladenosine RNA binding protein 1 (YTHDF1) is a key m6A reader involved in the development of GC [19, 20]. YTHDF1 has been reported to prevent the degradation of multiple target genes, such as *NOTCH1*, *EIF3C*, and *ATG14A*, by recognizing their m6A modifications [21–23]. However, the interaction between *SLC39A4* and YTHDF1 in GC is not yet clear.

The purpose of this study is to explore the relationship between *SLC39A4* and YTHDF1 and their effects on cuproptosis in the context of GC to reveal effective strategies for discouraging the progression of GC.

MATERIALS AND METHODS

Bioinformatics analysis

RNA sequencing data from GC patient samples were obtained from the GEO database (GSE103236, GSE56807, and GSE172032). Differentially expressed genes were identified using a threshold of $\log_2\text{FC} > 1$ and $P < 0.01$ [24–26]. The ENCORI database was used to retrieve m6A readers that bind to *SLC39A4* [27]. The potential m6A modification sites on *SLC39A4* were obtained from SRAMP database [28].

Patient samples

All patient samples were obtained from the Department of Pathology at the Second Affiliated Hospital of Harbin Medical University. Fifteen frozen GC tissue samples and paired para-carcinoma tissues from patients who had not undergone chemotherapy were used for molecular testing. Additionally, three paraffin-embedded GC tissue samples were used for immunohistochemical analysis to detect *SLC39A4* expression. All experimental procedures received approval from the Ethics Committee of the Second Affiliated Hospital of Harbin Medical University (No. YJSKY2024-376) and strictly adhered to the Declaration of Helsinki. This study obtained informed consent from all participants.

Cu^{2+} measurement

The Cu^{2+} level was measured using the Cu^{2+} Colorimetric Assay Kit (Elabscience, Wuhan, China). This method was based on the principle that Cu^{2+} dissociate in an acidic environment and form a purple complex upon chelation with 3,5-DiBr-PAESA. In brief, the samples were incubated with the color-developing solution at 37 °C for 5 min, and the optical density was examined at 580 nm.

Cell lines

Gastric epithelial cell lines GES-1 and GC cell lines AGS, HGC-27, MKN-45, NCI-N87, and SNU-16 were purchased from iCell (Shanghai, China) and

cultured at 37 °C, 5% CO_2 . The GES-1, MKN-45, NCI-N87, and SNU-16 cells were cultured in RPMI-1640 medium supplemented with 10% bovine serum albumin (BSA). The AGS and HGC-27 cells were cultured in F12K medium containing 10% fetal bovine serum and DMEM medium, respectively. The cell lines were verified via short tandem repeat (STR) profiling, and the supplier certified their mycoplasma-free status.

Cell treatment

AGS and MKN-45 cells were treated with medium containing 1 μM CuCl_2 (Macklin, Shanghai, China) supplemented with varying concentrations of elesclomol (EC) (Macklin, Shanghai, China) at 0, 10, 25, 50, 100, 200, and 400 nM to induce cuproptosis. After 48 h, cell viability was tested via the CCK-8 method, with the half-maximal inhibitory concentration (IC50) calculated accordingly. Based on the IC50 values, 1 μM CuCl_2 and 50 nM EC were selected for subsequent experiments.

Plasmid transfection

The coding sequence (CDS) of *SLC39A4* was ligated into the pcDNA3.1 plasmid, while the short hairpin RNA (shRNA) targeting *SLC39A4* was cloned into the pRNAH1.1 plasmid. The recombinant plasmids were transfected into AGS and MKN-45 cells using Lipofectamine 3000 transfection reagent. After 48 h, stably transfected cells were selected using 200 mg/ml G418. Subsequently, the stable cells underwent monoclonal culture, and the expression of *SLC39A4* protein and mRNA was assessed to identify monoclonal cells exhibiting the most effective overexpression or knockdown for subsequent experiments. Additionally, the CDS of *YTHDF1* was cloned into the pcDNA3.1 plasmid and transiently transfected into AGS and MKN-45 cells.

mRNA stability assay

After transfection with the plasmid for 48 h, the cells were exposed to 5 $\mu\text{g}/\text{mL}$ Actinomycin D for varying durations (0, 2, 4, and 6 h), followed by collection and subsequent real-time qPCR analysis.

Real-time qPCR

First-strand cDNA synthesis was carried out on the total RNA sample, employing an All-in-One First-Strand SuperMix according to the manufacturer's instructions. Real-time qPCR was performed with SYBR Green dye on a PANGAEA 3 fluorometric quantifier. The specific primer sequences used are as follows. *Homo SLC39A4*, (forward) 5'-GAGCGGGTCTTGCTTCCA-3', (reverse) 5'-GCACCTCAGGCATACCGTGTC-3'. *Homo YTHDF1*, (forward) 5'-AACCCGAAAGAGTTTGAGTG-3', (reverse) 5'-GCTGAAGAGCAGGTAGACG-3'.

Western blot

The total proteins were loaded onto SDS-PAGE for separation and subsequently transferred to PVDF membranes. The membranes were blocked with a commercial blocking buffer and incubated with *SLC39A4* antibody (Cat. No. 20625-1-AP, Proteintech, Rosemont, IL, USA), YTHDF1 antibody (Cat. No. 17479-1-AP, Proteintech), FDX1 antibody (Cat. No. 12592-1-AP, Proteintech), lipoic acid antibody (for the detection of DLAT lipoylation) (Cat. No. ab58724, Abcam, Boston, MA, USA), DLAT antibody (Cat. No. 12362, Cell Signaling Technology, Danvers, MA, USA), and GAPDH antibody (Cat. No. 60004-1-Ig, Proteintech) overnight at 4 °C. Subsequently, the membranes were subjected to incubation with a secondary antibody conjugated to horseradish peroxidase (HRP) (Cat. No. SE134 & Cat. No. SE131, Solarbio, Beijing, China). The blots were subjected to enhanced chemiluminescence (ECL) detection, and the resulting signals were acquired using a chemiluminescence imaging system. The gray values were analyzed using Tanon Image software (Shanghai, China).

Immunohistochemistry

Paraffin sections were dewaxed and boiled in an antigen retrieval solution. The sections were subjected to hydrogen peroxide (3%) incubation and BSA (1%) blocking. Sections were then incubated overnight at 4 °C with *SLC39A4* (Cat. No. 20625-1-AP, Proteintech) and FDX1 (Cat. No. 12592-1-AP, Proteintech) antibodies, followed by incubation with an HRP-labeled secondary antibody (Cat. No. 31460, Thermo Scientific, Pittsburgh, PA, USA). Finally, hematoxylin counterstaining was applied following DAB incubation to the sections.

5-ethynyl 2'-deoxyuridine (EdU) staining

A Click-iT EdU-488 Cell Proliferation Test Kit (Biosharp, Hefei, China) was used. Cells (2.0×10^4) were incubated in EdU staining solution for 2 h,

followed by incubation with Click-iT reaction solution for 30 min. Hoechst 33342 was used for nuclear staining. Fluorescence intensity was measured by flow cytometry.

Cell cycle

A Cell Cycle Assay Kit was obtained from Biosharp. After fixation in 70% ethanol, the cells were resuspended and treated with a solution containing propidium iodide (PI) and RNase A. Fluorescence intensity was measured using flow cytometry.

Colony formation

The cells were resuspended in complete medium and reseeded at a density of 250 cells per well. Following a 12-day culture period, the cells were fixed using 4% paraformaldehyde and subsequently stained with crystal violet.

Animals

Four-week-old male BALB/c nude mice were randomly divided into 12 groups. Although no formal statistical power analysis was conducted, the number of animals per group ($n = 6-8$) was determined based on previous studies using xenograft tumor models, adhering to the principle of minimizing animal use while ensuring reproducibility. Five million (5×10^6) cells were injected subcutaneously into each mouse. Tumor diameter was measured every three days. Mice that developed tumors within 10 days after cell injection were included in the study, while those that did not develop tumors were excluded. Intraperitoneal injections of 25 mg/kg EC were administered three times per week for three weeks to induce cuproptosis. The mice were euthanized after 28 days, and tumor tissues were harvested for analysis. To assess the outcomes, authors who were not involved in the experiments were asked to evaluate the results in a blinded manner. The animal experiments were approved by the Ethics Committee of the Second Affiliated Hospital of Harbin Medical University (No. YJSDW2024-189).

RNA immunoprecipitation (RIP)-PCR

An EZ-Magna RIP RNA-Binding Protein Immunoprecipitation Kit was obtained from Millipore (Billerica, MA, USA). Magnetic beads were incubated with YTHDF1 antibodies, after which cell lysates were added to the bead-antibody complex to precipitate RNA. Subsequently, the magnetic beads were separated using a magnetic rack, and proteins were digested with proteinase K to isolate RNA. The RNA was then amplified by PCR and analyzed using agarose gel electrophoresis. The primer sequence is as follows. *Homo SLC39A4*, (forward) 5'-CGATGTTGAAAGTACGG-3', (reverse) 5'-TCCAAGGACAAGAGTGTC-3'.

Dual-luciferase reporter gene assay

The luciferase reporter plasmid was constructed by inserting either the mutant (MUT) or wild-type (WT) sequence, and was co-transfected with a YTHDF1 overexpression plasmid into MKN-45 cells. Activity from the co-transfected Renilla luciferase plasmid was used for normalization. Assessment of fluorescence intensity was performed following a 48-h incubation, utilizing a commercial Luciferase Assay Kit.

Phosphorylation proteomics

Phosphorylation proteomics analysis was performed by Spec Ally Life Technology Co. (Wuhan, China). Briefly, proteins were reduced, alkylated, and then digested enzymatically using trypsin. (Dithiothreitol and iodoacetamide were used for reduction and alkylation, respectively.) Following enzymatic digestion, peptide samples were loaded onto a C18 microcolumn for desalting and then vacuum-dried. The peptide fractions were then bound to a StageTip microcolumn to enrich phosphorylated peptides. Peptide segments were characterized using a coupled liquid chromatography and tandem mass spectrometry (LC-MS/MS) system. The phosphorylated peptides were dissolved in buffer and separated using the EASY-nLC 1200 system equipped with a C18 column (Thermo Scientific). MS data were acquired using the Orbitrap Exploris 480 mass spectrometer (Thermo Scientific). The MS data were analyzed with MaxQuant software and searched against the SwissProt protein database. The functional enrichment of pathways was assessed via the Kyoto Encyclopedia of Genes and Genomes (KEGG) database, utilizing the clusterProfiler package in R.

Statistical analysis

The mean and standard deviation (mean \pm SD) are used to present the results. All data underwent normality tests and evaluation of homogeneity

of variances between groups prior to statistical analysis. For comparisons involving two groups, the F-test was used to assess equality of variances. For multiple groups, the Brown-Forsythe test was applied. When data failed to meet the assumption of normal distribution or when the assumption of homogeneity of variance was violated, equivalent nonparametric tests were employed (Mann-Whitney U test instead of the independent samples *t*-test, and Kruskal-Wallis test instead of one-way ANOVA). Data that conform to a normal distribution and pass the homogeneity of variance test were analyzed using parametric tests. We employed the Student's *t* test for two-group comparisons. For multi-group analyses, one-way or two-way ANOVA was conducted, and significant outcomes were further examined with Tukey's post hoc test. Statistical significance was defined as a *p*-value below 0.05.

RESULTS

High levels of SLC39A4 in tumor tissues of GC patients predicted poor prognosis

The GSE56807, GSE103236, and GSE172032 datasets provide mRNA sequencing data from cancer tissues and adjacent normal tissue samples of GC patients. To pinpoint key genes governing GC progression, differential expression analysis was performed on these datasets (Fig. 1A). The differentially expressed genes in the GSE56807, GSE103236, and GSE172032 datasets were analyzed using a threshold of $\log_2FC > 1$ and $P < 0.01$ (Supplementary Fig. S1A). Ninety-five candidate genes were identified by screening the common genes among the differentially expressed genes across three GSE datasets, as well as genes associated with GC (Supplementary Fig. S1B). Through an extensive literature review, we focused on *SLC39A4*, a gene that was highly expressed in GC tissues (Supplementary Fig. S1C). The analysis results from the TNMplot and cProSite websites indicated that the expression of *SLC39A4* was elevated at both the transcriptional and translational levels (Fig. 1B, C) in GC. High *SLC39A4* expression levels were associated with poorer clinical outcomes in gastric cancer, including shorter overall survival, first progression survival, and post-progression survival, as assessed through the Kaplan-Meier Plotter platform (Fig. 1D-F). Cancer tissues from patients with GC exhibit elevated levels of Cu^{2+} compared to adjacent normal tissues (Fig. 1G), potentially contributing to tumor growth. Additionally, increased expression of *SLC39A4* was observed in cancer tissues, consistent with findings from database analysis (Fig. 1H-J). Compared with gastric epithelial cell line, GC cell lines exhibited increased expression of *SLC39A4* (Fig. 1K, L). In this study, we selected the GC cell lines AGS and MKN-45, which exhibit moderate levels of *SLC39A4* expression, allowing for both overexpression and knockdown of *SLC39A4* in these lines.

Screening of monoclonal cell lines for stable transfected cells

According to the results of real-time qPCR analysis (Supplementary Fig. S2A), For the AGS cell line, clones 4 and 43 were established with overexpression of *SLC39A4*, whereas clones 11 and 8 were generated with knockdown of *SLC39A4*. Similarly, in the MKN-45 cell line, clones 9 and 48 expressed elevated levels of *SLC39A4*, while clones 2 and 5 exhibited silenced expression of *SLC39A4*. The protein expression of *SLC39A4* in the selected clones was also examined using western blotting (Supplementary Fig. S2B).

SLC39A4 enhanced the proliferation of GC cells in vitro and in vivo

The results of the CCK-8 assay (Fig. 2A-D) demonstrate that *SLC39A4* upregulation drives the growth of GC cells, whereas silencing *SLC39A4* produces the opposite effect. Additionally, DNA replication activity in GC cells was analyzed using the EdU assay (Fig. 2E-H). *SLC39A4* overexpression increased the proportion of EdU-positive cells, indicating that *SLC39A4* promotes DNA replication. Conversely, *SLC39A4* knockdown inhibited this process (scatter plots are shown in Supplementary Fig. S3A). Cell cycle

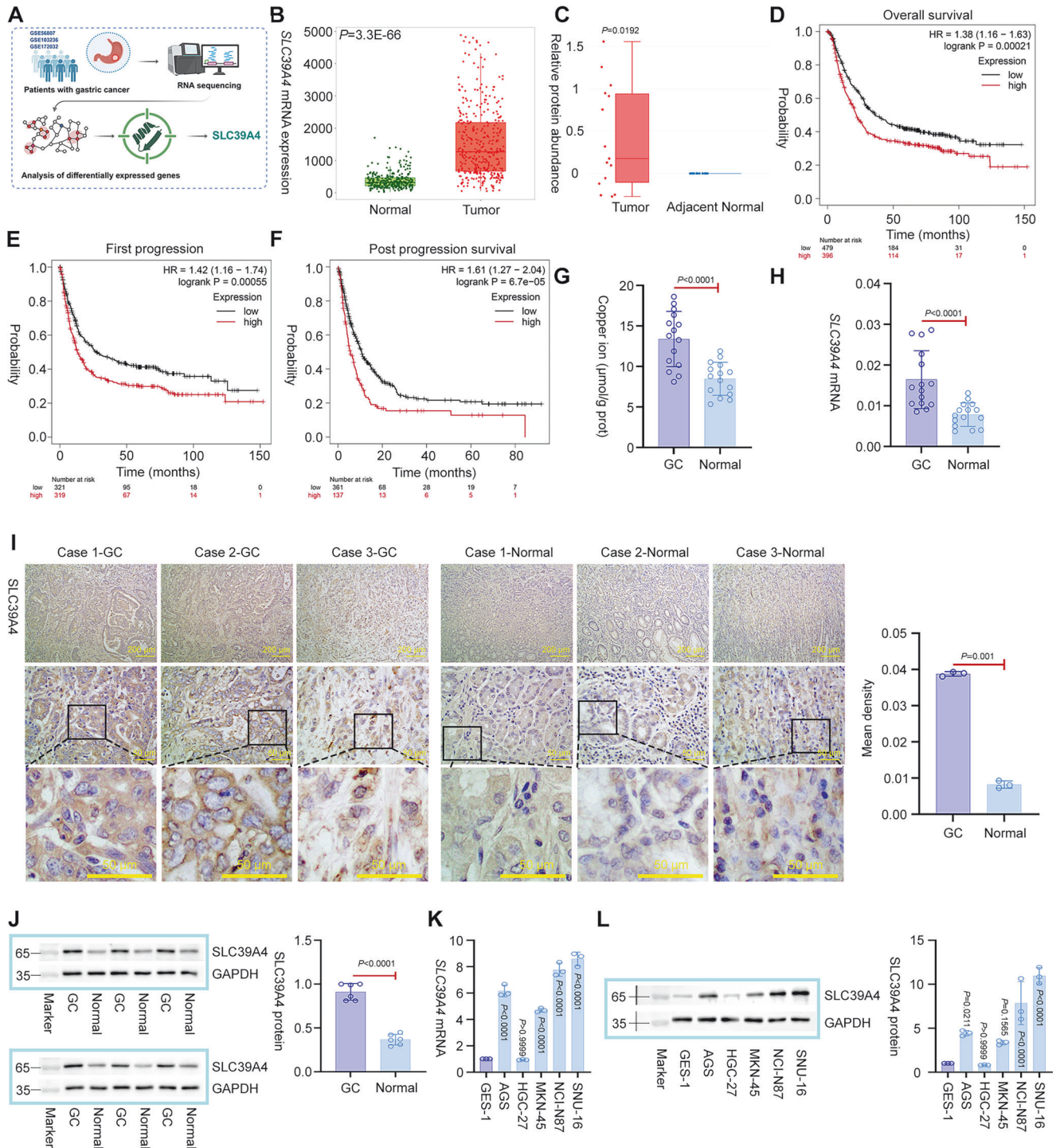


Fig. 1 SLC39A4 was highly expressed in tumor tissues of GC patients and predicted poor prognosis. **A** This study conducted a comprehensive analysis of differentially expressed genes in the tumor tissues of GC patients using the datasets GSE56807, GSE103236, and GSE172032 from the GEO database, with a particular focus on SLC39A4. The diagram was generated by BioRender (<https://www.biorender.com/>). **B** SLC39A4 mRNA expression in GC patient samples from TNM-plot website. **C** SLC39A4 protein expression in GC patient samples from cProSite website. The relationship between SLC39A4 expression and overall survival (**D**), first progression survival (**E**), and post progression survival (**F**) in patients with GC was analyzed using the KM-plotter website. **G** Copper ion level in the samples collected from patients with GC. $N=15$. **H** SLC39A4 mRNA expression in the patient samples. $N=15$. **I** Representative SLC39A4 immunohistochemical staining images in the tumor tissues of patient samples. $N=3$. **J** SLC39A4 protein expression in the patient samples. $N=6$. SLC39A4 mRNA expression (**K**) and protein expression (**L**) in GC cell lines and gastric epithelial cell line GES-1. $N=3$. GC, gastric cancer; SLC39A4, Solute carrier family 39 member 4. The data is presented as the mean value \pm standard deviation, and $p < 0.05$ was considered statistically significant.

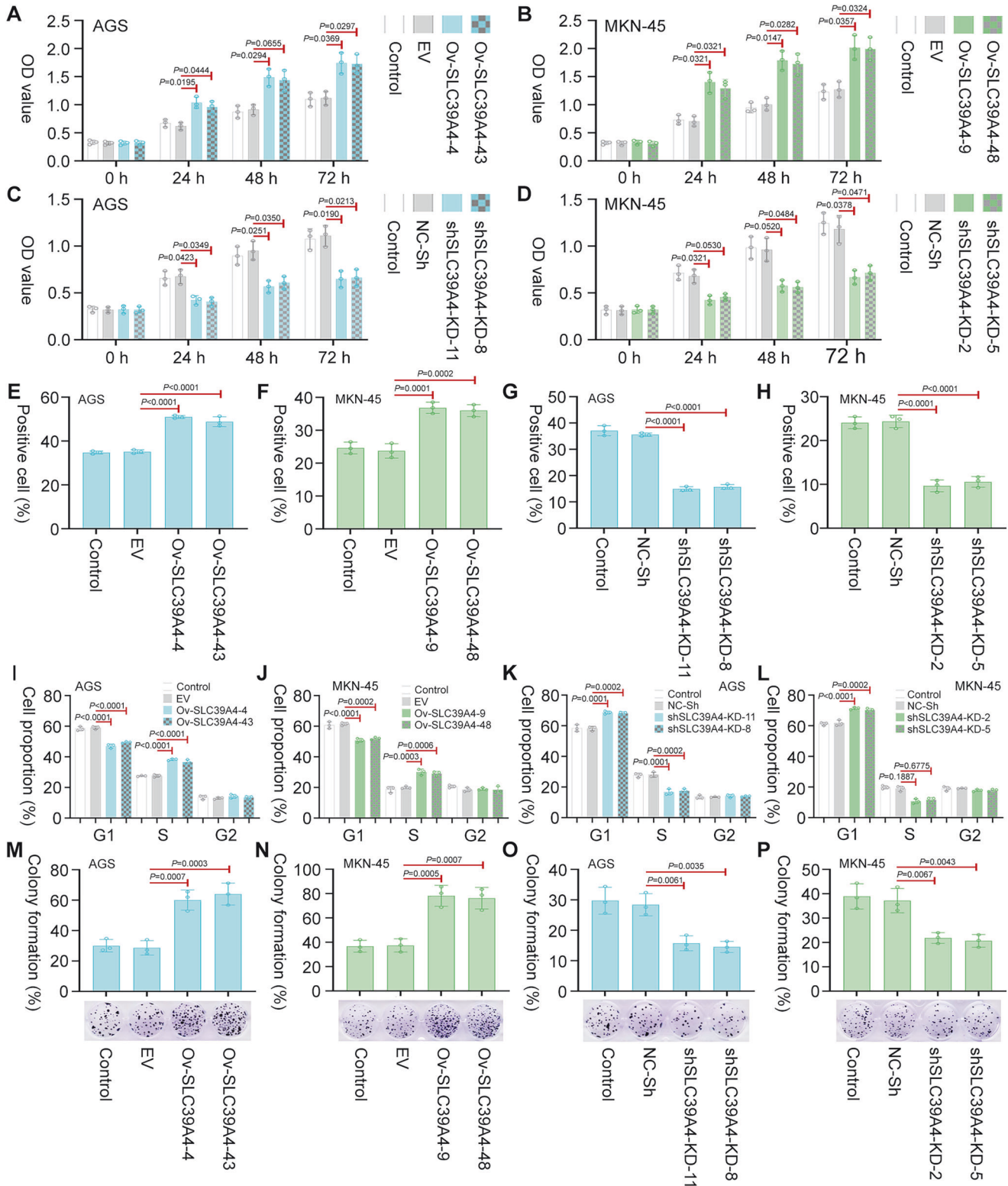


Fig. 2 SLC39A4 promoted the proliferation of GC cells. **A, B** Cell proliferation in SLC39A4-overexpressed monoclonal strains. **C, D** Cell proliferation in SLC39A4-silenced monoclonal strains. Cell proliferation in SLC39A4-overexpressed (**E, F**) and SLC39A4-silenced (**G, H**) GC cells was examined using EdU staining and analyzed using flow cytometry. Cell cycle in SLC39A4-overexpressed (**I, J**) and SLC39A4-silenced (**K, L**) was analyzed using flow cytometry. Clone formation in SLC39A4-overexpressed (**M, N**) and SLC39A4-silenced (**O, P**). $N = 3$. SLC39A4 Solute carrier family 39 member 4, GC gastric cancer, EdU 5-ethynyl-2-deoxyuridine, OD optical density, NC-Sh negative control short hairpin RNA sequence, shSLC39A4-KD-11/8/2/5 monoclonal 11/8/2/5 that was transfected with a short hairpin RNA sequence targeting SLC39A4, EV empty vector, Ov-SLC39A4-4/43/9/48 monoclonal 4/43/9/48 that was transfected with a SLC39A4 overexpression plasmid. The data is presented as the mean value \pm standard deviation, and $p < 0.05$ was considered statistically significant.

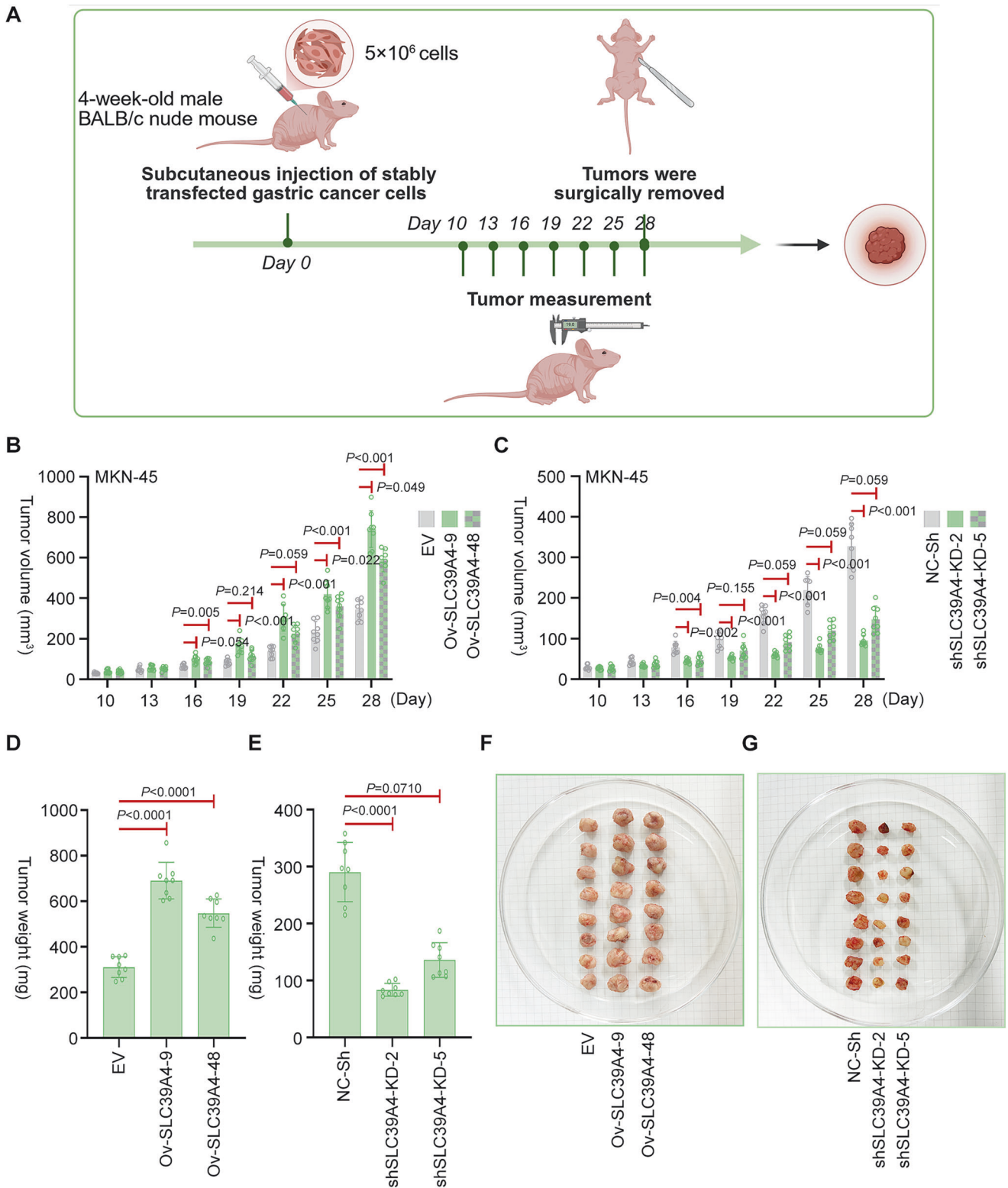


Fig. 3 SLC39A4 accelerated the growth of GC cells in xenograft models. **A** MKN-45 cells were injected subcutaneously into nude mice, and tumor tissues were collected 28 days later. The diagram was generated by BioRender (<https://www.biorender.com/>). Changes in tumor volume of the mice received SLC39A4-overexpressed cells (**B**) and SLC39A4-silenced cells (**C**). Tumor weight of the mice received SLC39A4-overexpressed cells (**D**) and SLC39A4-silenced cells (**E**). Images of tumor tissues formed by SLC39A4-overexpressed cells (**F**) and SLC39A4-silenced cells (**G**). $N = 8$. SLC39A4 Solute carrier family 39 member 4, GC gastric cancer, NC-Sh negative control short hairpin RNA sequence, shSLC39A4-KD-2/5 monoclonal 2/5 that was transfected with a short hairpin RNA sequence targeting SLC39A4, EV empty vector, Ov-SLC39A4-9/48 monoclonal 9/48 that was transfected with a SLC39A4 overexpression plasmid. The data is presented as the mean value \pm standard deviation, and $p < 0.05$ was considered statistically significant.

analysis yielded results consistent with those of the EdU assay (Fig. 2I–L). SLC39A4 overexpression accelerated the G1/S phase progression in GC cells, while its knockdown induced G1 phase arrest (histograms are shown in Supplementary Fig. S3B). In addition, overexpression of SLC39A4 enhanced the colony formation of GC cells, whereas SLC39A4 silencing produced the opposite effect (Fig. 2M–P).

Evidence from *in vivo* experiments also supports the oncogenic function of SLC39A4 (Fig. 3A). *In vivo* studies utilizing MKN-45 cell-based xenografts demonstrated an oncogenic function for SLC39A4. Gain- and loss-of-function studies confirmed that its overexpression enhanced tumor growth, while its knockdown attenuated tumor development (Fig. 3B, C). At the experimental endpoint, tumor weight increased in the SLC39A4 overexpression group, whereas it decreased in the SLC39A4 knockdown group (Fig. 3D, E). This trend was also evident in the images of the tumor tissues (Fig. 3F, G).

SLC39A4 enhanced resistance to cuproptosis *in vitro* and *in vivo*

To define the contribution of SLC39A4 to cuproptosis in GC, we exposed stably transfected GC cells to CuCl₂ along with increasing doses of EC. The results indicated that high levels of SLC39A4 promoted cell proliferation, whereas knockdown of SLC39A4 inhibited GC cell survival and accelerated cuproptosis (Fig. 4A–D). The IC₅₀ of EC on GC cells was ~50 nM. Therefore, CuCl₂ and 50 nM EC were selected as cuproptosis inducers for the subsequent experiments. Elevated levels of FDX1 and increased acylation of DLAT indicate the occurrence of cuproptosis. Overexpression of SLC39A4 inhibited FDX1 expression and DLAT lipoylation, whereas silencing SLC39A4 further enhanced the levels of cuproptosis markers (Fig. 4E–H). The formation of DLAT oligomers, another marker of cuproptosis, was examined using immunofluorescence microscopy (Fig. 4I, J). The results showed that overexpression of SLC39A4 reduced DLAT oligomer formation, whereas knockdown of SLC39A4 further increased the production of DLAT oligomers.

In the xenograft model, overexpression of SLC39A4 reversed EC-induced cuproptosis, whereas SLC39A4 knockdown combined with EC treatment synergistically inhibited tumor growth (Fig. 5A–D), as also evidenced by the tumor images (Fig. 5E, F). The inhibitory effect of SLC39A4 on cuproptosis was demonstrated *in vivo* by measuring the expression of FDX1, a marker of cuproptosis (Fig. 5G). Furthermore, we obtained immunohistochemical staining images of FDX1 in tumor tissues from GC patients using the Human Protein Atlas (HPA) database (Fig. 5H). These images showed low FDX1 expression, indicating a reduced level of cuproptosis in GC patients.

YTHDF1 overexpression enhanced resistance to cuproptosis *in vivo*

Compared with adjacent non-cancerous tissues, YTHDF1 showed significantly higher expression in GC specimens (Fig. 6A). Figure 6B–D shows that overexpression of YTHDF1 reversed the anti-growth effect of elesclomol following xenotransplantation of GC cells. Furthermore, YTHDF1 overexpression suppressed cuproptosis in GC, as demonstrated by the decreased expression of the cuproptosis markers FDX1 and lip-DLAT (revised Fig. 6E).

YTHDF1 enhanced SLC39A4 mRNA stability via reading m6A modification

Analysis of the ENCORI database indicates that SLC39A4 may interact with multiple m6A readers (Supplementary Fig S4A). A positive correlation was observed between the mRNA level of SLC39A4 and the m6A reader YTHDF1. Additionally, the expression levels of YTHDF1 and SLC39A4 were positively correlated in samples from GC patients (Fig. 7A). Furthermore, YTHDF1 has multiple potential binding sites within the CDS and the 3'-

untranslated region (3'-UTR) of SLC39A4. Based on the evidence presented above, this study further investigates the regulation of SLC39A4 expression by YTHDF1. The YTHDF1 overexpression plasmid was transfected into GC cells. YTHDF1 was successfully expressed in GC cells (Fig. 7B–E). Overexpression of YTHDF1 promoted the expression of SLC39A4 (Fig. 7F–I), potentially by preventing the degradation of SLC39A4 mRNA (Fig. 7J). RIP-PCR analysis confirmed that YTHDF1 binds directly to SLC39A4 mRNA (Fig. 7K). The SRAMP database analysis revealed that YTHDF1 preferentially binds to the GGACC motif, which is located within the binding sequence of YTHDF1 on the SLC39A4 mRNA, as predicted by the ENCORI database (Supplementary Fig. S4B). Therefore, the dual-luciferase reporter vector was constructed to harbor the CDS of SLC39A4, in which alanine at position 1962 was mutated to cysteine. The results showed that YTHDF1 interacted with the wild-type SLC39A4 sequence, whereas the m6A site mutant SLC39A4 was not regulated by YTHDF1 expression (Fig. 7L). The findings indicate that YTHDF1 may stabilize the mRNA expression of SLC39A4 by recognizing the m6A modification within the CDS.

Overexpression of SLC39A4 affected protein phosphorylation modifications in GC cells treated with EC-Cu

To investigate the downstream mechanisms through which SLC39A4 regulates cuproptosis, we conducted a phosphorylation proteomics analysis of proteins in SLC39A4-overexpressing GC cells treated with EC-Cu. Upregulation of SLC39A4 increased the phosphorylation levels of 11 downstream proteins while concurrently decreasing the phosphorylation levels of 107 downstream proteins (Supplementary Fig. S5A). These proteins primarily participate in the MAPK, TNF, and the cGMP-PKG signaling pathway (Supplementary Fig. S5B). Furthermore, we analyzed the phosphorylation site motifs of differentially phosphorylated peptides (Supplementary Fig. S5C–H), and observed that the overexpression of SLC39A4 primarily affected serine (S) phosphorylation. The kinase-substrate enrichment analysis (KSEA) identified that kinases, including CSNK2A1, MAPK1, PRKACA, CDK1, and MAPK3, were activated in GC cells overexpressing SLC39A4 (Supplementary Fig. S5I). The increased expression of phosphorylated HSPB1 (p-HSPB1) in GC cell lines treated with SLC39A4 overexpression and EC-Cu was confirmed (Supplementary Fig. S5J).

DISCUSSION

Copper is an essential metallic element that plays a crucial role in various physiological processes, including the promotion of tumor growth and invasion. However, excessive Cu²⁺ can induce a form of cell death known as cuproptosis [6]. The application of elevated copper ion concentrations to induce cuproptosis is considered a promising therapeutic strategy for GC [29]. SLC39A4 undergoes m6A modification in its mRNA, which is recognized by YTHDF1 to stabilize SLC39A4 mRNA. This stabilization inhibits the expression of FDX1, thereby suppressing the downstream cascade of reactions related to cuproptosis and promoting the progression of GC. Targeting SLC39A4 enhances the induction of cuproptosis in GC cells. The combination of SLC39A4 silencing and the cuproptosis inducer EC represents a potential therapeutic strategy for GC. This study broadens our understanding of GC treatment strategies that induce cuproptosis at the molecular level, offering a novel and promising molecular target for GC therapy.

Upregulation of SLC39A4 has been observed in esophageal squamous cell carcinoma [30], hepatocellular carcinoma [10], and pancreatic cancer [31], where it contributes to cancer progression. This indicates that SLC39A4 is a potential oncogene. However, a comprehensive understanding of its role in GC is still lacking. Upregulation of SLC39A4 was identified in GC and linked to

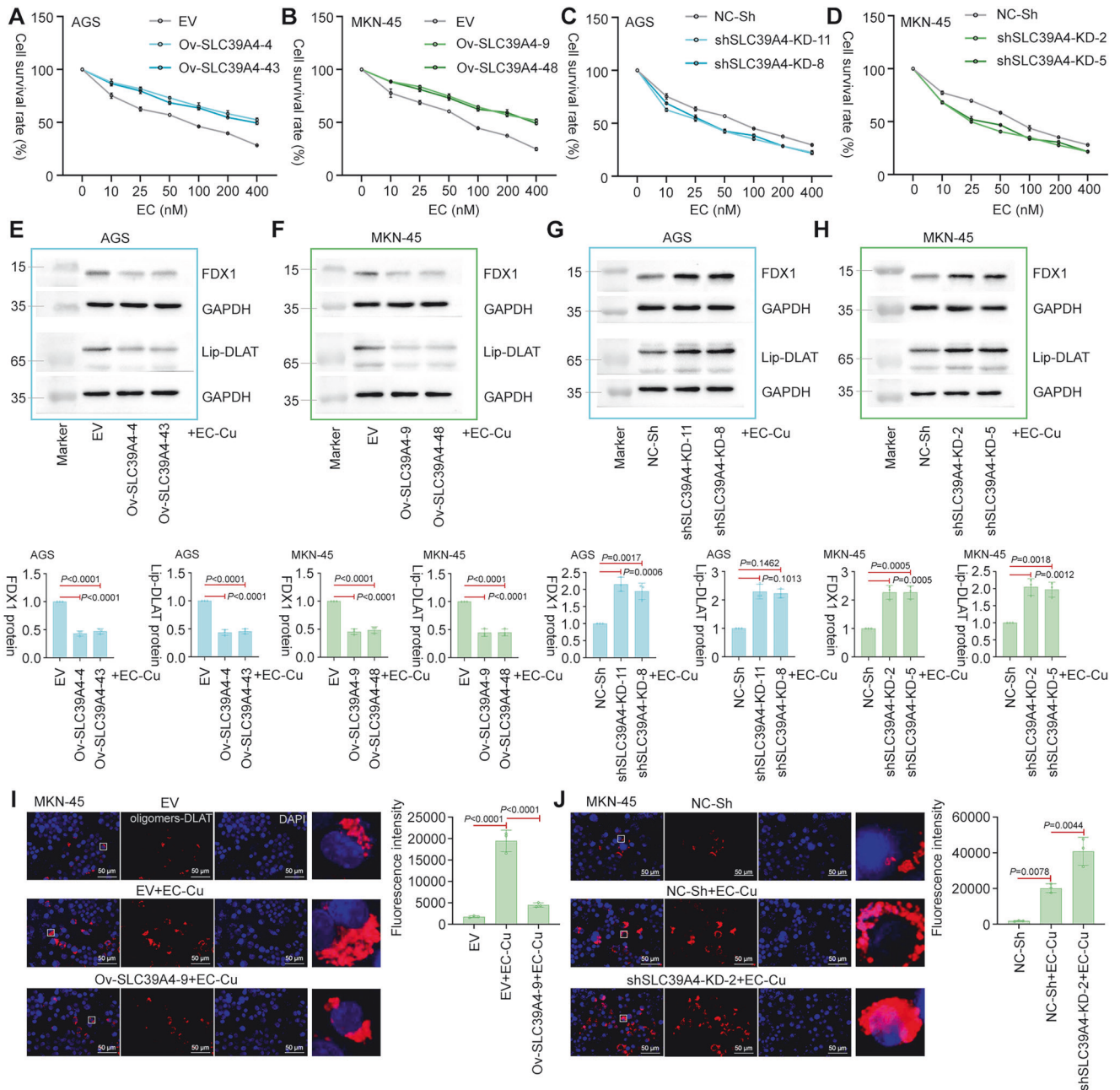


Fig. 4 SLC39A4 enhanced resistance to cuproptosis in GC cells. The GC cells were treated with $1 \mu\text{M}$ CuCl_2 and different concentrations of elesclomol for 48 h. Cell survival rate in SLC39A4-overexpressed (**A**, **B**) and SLC39A4-silence (**C**, **D**) cells. Protein expression of cuproptosis markers FDX1 and Lip-DLAT in SLC39A4-overexpressed (**E**, **F**) and SLC39A4-silenced (**G**, **H**) cells. Representative oligomers-DLAT immunofluorescence staining images of SLC39A4-overexpressed (**I**) and SLC39A4-silenced (**J**) cells. $N = 3$. SLC39A4 Solute carrier family 39 member 4, GC gastric cancer, EC elesclomol, Cu copper, FDX1 ferredoxin 1, DLAT dihydrolipoamide S-acetyltransferase, Lip-DLAT lipoylation of dihydrolipoamide S-acetyltransferase, DAPI 4', 6-diamidino-2-phenylindole, NC-Sh negative control short hairpin RNA sequence, shSLC39A4-KD-11/8/2/5 monoclonal 11/8/2/5 that was transfected with a short hairpin RNA sequence targeting SLC39A4, EV empty vector, Ov-SLC39A4-4/43/9/48 monoclonal 4/43/9/48 that was transfected with a SLC39A4 overexpression plasmid. The data is presented as the mean value \pm standard deviation, and $p < 0.05$ was considered statistically significant.

unfavorable clinical outcomes. Silencing SLC39A4 inhibits the proliferation of GC cells both in vivo and in vitro. These findings fill the gap in understanding the function of SLC39A4 in GC and further clarify its role as a cancer-promoting gene. Importantly, the knockdown of SLC39A4 has been found to increase the protein expression of key cuproptosis markers, FDX1 and DLAT in intrahepatic cholangiocarcinoma [14]. This finding strongly supports the focus of this study in exploring the key genes involved in cuproptosis within the context of cancer. In addition, the study

demonstrated that SLC39A4 can bind and transport Cu^{2+} , rather than being limited to Zn^{2+} as previously believed [9]. Therefore, we speculate that the inhibitory effect of SLC39A4 on cuproptosis may also be applicable to GC. This study reports that SLC39A4 confers resistance to EC-induced cuproptosis. Knockdown of SLC39A4 synergistically enhances cuproptosis in GC cells treated with EC, as demonstrated by increased expression of FDX1 and lipid acylation of DLAT. These findings align with previous research.

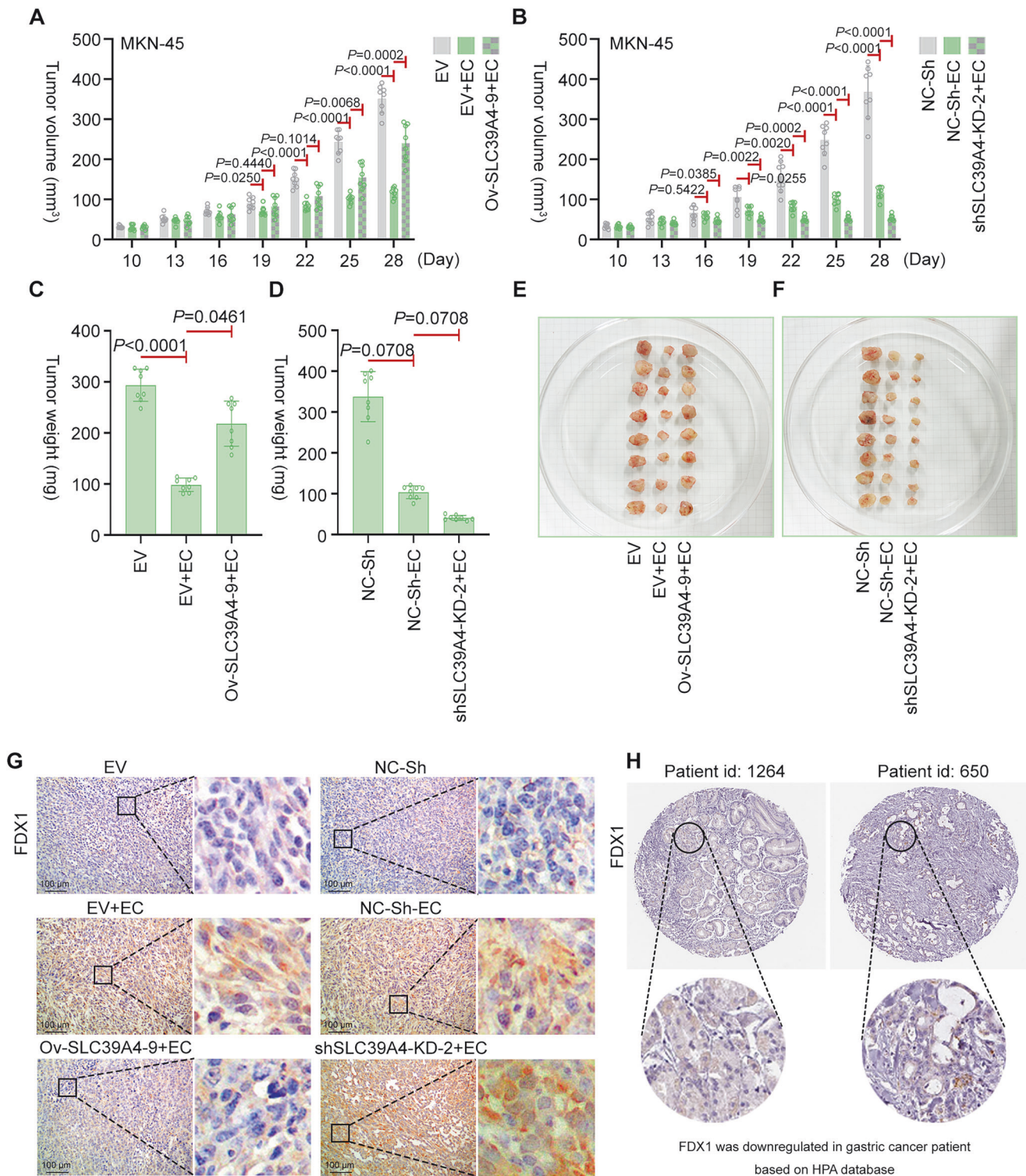


Fig. 5 SLC39A4 enhanced resistance to cuproptosis of GC cells in xenograft models. Xenografted mice received intraperitoneal injection of elesclomol, and tumor tissues were collected 28 days later. Changes in tumor volume of the mice received SLC39A4-overexpressed cells (A) and SLC39A4-silenced cells (B). Tumor weight of the mice received SLC39A4-overexpressed cells (C) and SLC39A4-silenced cells (D). Images of tumor tissues formed by SLC39A4-overexpressed cells (E) and SLC39A4-silenced cells (F). G Representative FDX1 immunohistochemical staining images in tumor tissues. H FDX1 immunohistochemical staining images in GC patients from HPA database. $N = 8$. SLC39A4 Solute carrier family 39 member 4, GC gastric cancer, EC elesclomol, Cu copper, FDX1 ferredoxin 1, HPA human protein atlas, NC-Sh negative control short hairpin RNA sequence, shSLC39A4-KD-2 monoclonal 2 that was transfected with a short hairpin RNA sequence targeting SLC39A4, EV empty vector, Ov-SLC39A4-9 monoclonal 9 that was transfected with a SLC39A4 overexpression plasmid. The data is presented as the mean value \pm standard deviation, and $p < 0.05$ was considered statistically significant.

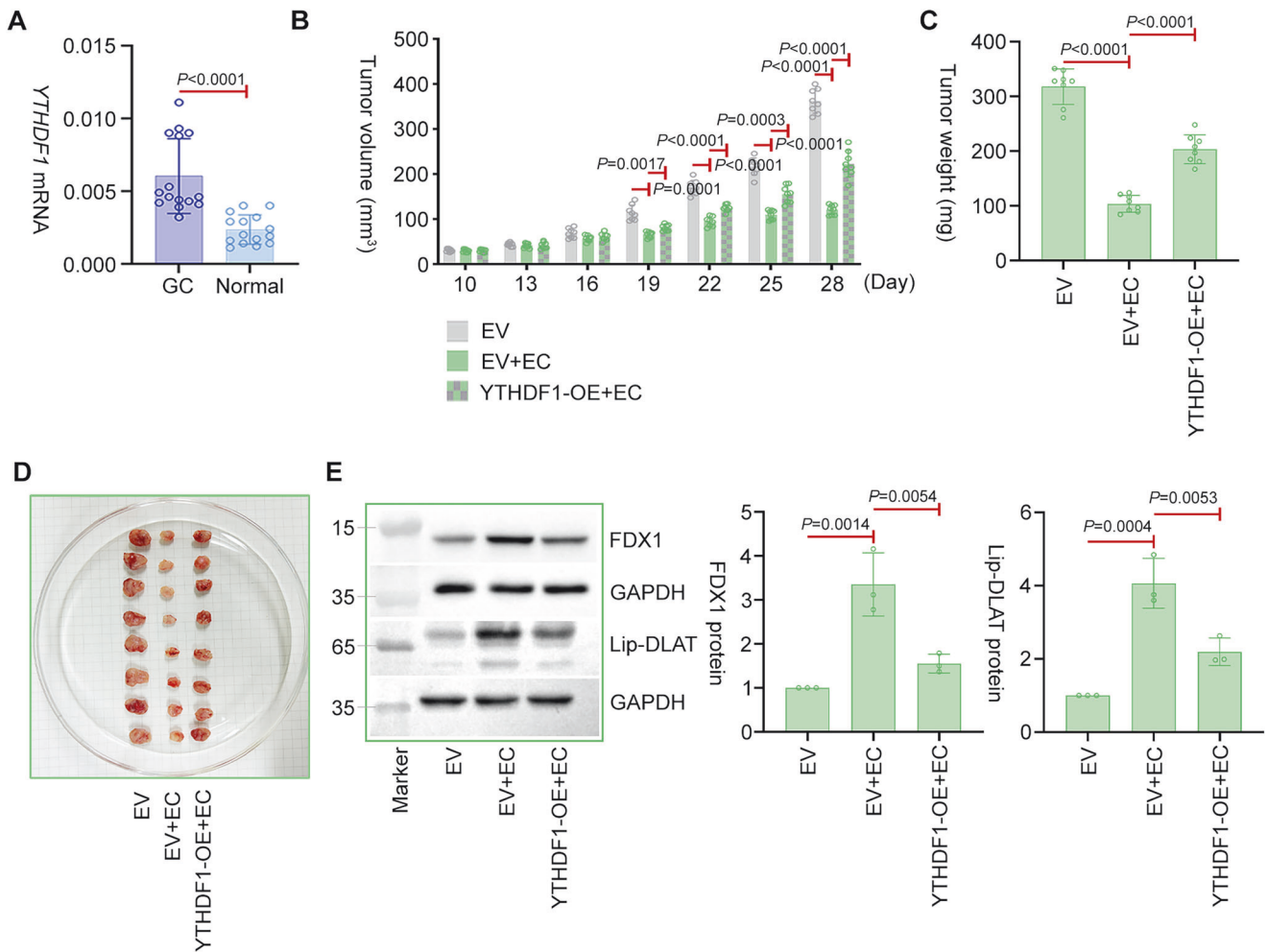


Fig. 6 YTHDF1 overexpression enhanced resistance to cuproptosis of GC cells in xenograft models. **A** YTHDF1 mRNA expression in the samples collected from patients with GC. Xenografted mice received intraperitoneal injection of elesclomol, and tumor tissues were collected 28 days later. Changes in tumor volume of the mice received YTHDF1-overexpressed cells (**B**). Tumor weight of the mice received YTHDF1-overexpressed cells (**C**). Images of tumor tissues formed by YTHDF1-overexpressed cells (**D**). **E** Protein expression of cuproptosis markers FDX1 and Lip-DLAT in tumor tissues. $N = 8$. YTHDF1 YTH N6-methyladenosine RNA binding protein F1, GC gastric cancer, EC elesclomol, FDX1 ferredoxin 1, Lip-DLAT lipoylation of dihydrolipoamide S-acetyltransferase, EV empty vector, YTHDF1-OE YTHDF1 overexpression plasmid. The data is presented as the mean value \pm standard deviation, and $p < 0.05$ was considered statistically significant.

YTHDF1, an m6A reader, was also shown to be upregulated in GC tissues and to enhance the resistance of GC cells to cuproptosis. YTHDF1 is a known promoter of GC and regulates multiple target genes by recognizing m6A modifications. As an m6A reader, YTHDF1 has been reported to promote the translation of FZD7, thereby activating the Wnt/ β -catenin signaling pathway and facilitating GC progression [32]. Furthermore, YTHDF1 also acts as an m6A reader to facilitate the translation of USP14 [33], TCF7 [34], and SCARB1 [35], thereby promoting the progression of GC. However, the interaction between YTHDF1 and SLC39A4 has not yet been fully elucidated. This study reveals that YTHDF1 enhances the stability of SLC39A4 mRNA and promotes its translation by recognizing m6A modification. Interestingly, it was observed that SLC39A4-MUT group exhibited almost the same luciferase activity as in the SLC39A4-MUT group with YTHDF1 overexpression. Under conditions of YTHDF1 overexpression, the factors influencing differences in the transcriptional levels of SLC39A4 between the SLC39A4-MUT and SLC39A4-WT groups include both the regulatory effect of YTHDF1 on m6A and the m6A modification itself. Previous studies have shown that m6A modification promotes transcriptional termination [36], and may lead to mRNA degradation through pathways mediated by m6A

readers, RNA-binding proteins, or cross-talk with other RNA modifications [37], which can partially inhibit gene transcription. In this study, although YTHDF1 overexpression enhanced the promoting effect of YTHDF1 on m6A-mediated SLC39A4 transcription, the inhibitory effect of m6A on transcription cannot be ignored. The A1952 mutation may eliminate the transcriptional inhibitory effect of m6A, which explains the observed high luciferase activity in the SLC39A4-MUT group. Similar results have also been reported in numerous studies [38, 39]. Apart from YTHDF1, analysis results from the ENCORI website suggest that several other m6A readers, such as IGF2BP1 and IGF2BP3, may also regulate the stability of SLC39A4 and thus warrant further attention. Additionally, the transcription factor UKLF has been shown to bind to SLC39A4, facilitating transcriptional activation [40]. This indicates that the expression of SLC39A4 is influenced not only by RNA m6A modification but may also be regulated at the transcriptional level.

In addition, the inhibitory effect of SLC39A4 on cuproptosis may be mediated through the regulation of specific signaling pathways. Activation of the PI3K/AKT pathway by SLC39A4 drove the malignant phenotype in nasopharyngeal carcinoma cells [17]. Additionally, the PI3K/AKT signaling pathway, when activated,

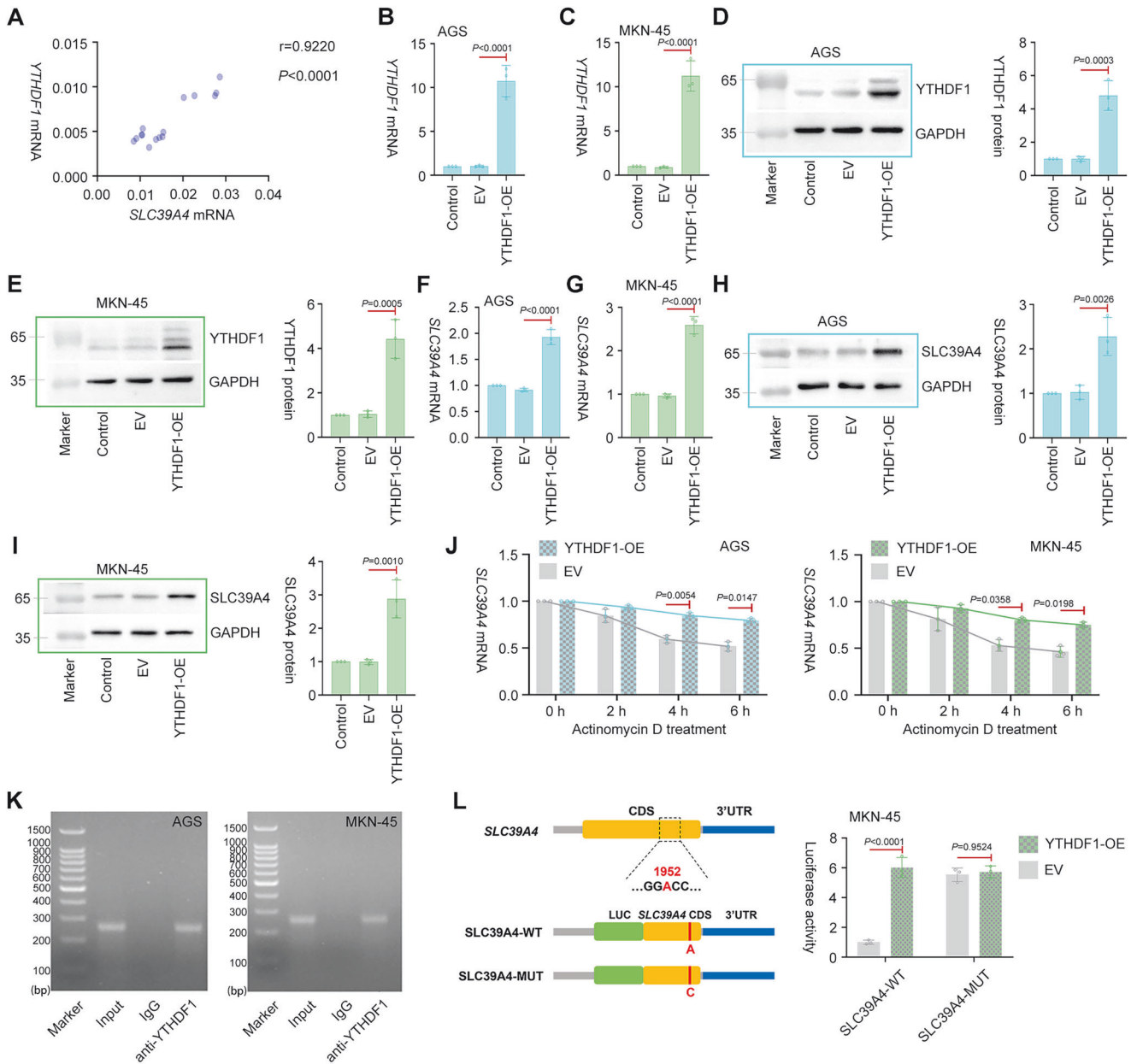


Fig. 7 YTHDF1 enhanced the stability of *SLC39A4* mRNA in an m⁶A dependent manner. **A** Correlation analysis of mRNA expression of *YTHDF1* and *SLC39A4* in clinical samples of GC patients. $N = 15$. *YTHDF1* overexpression plasmid was transfected into GC cells, and the following experiments were performed 48 h later. **B**, **C** *YTHDF1* mRNA expression in *YTHDF1*-overexpressed cells. **D**, **E** *YTHDF1* protein expression in *YTHDF1*-overexpressed cells. **F**, **G** *SLC39A4* mRNA expression in *YTHDF1*-overexpressed cells. **H**, **I** *SLC39A4* protein expression in *YTHDF1*-overexpressed cells. GC cells were treated with 5 μ g/mL Actinomycin D for 6 h. **J** *SLC39A4* mRNA expression in *YTHDF1*-overexpressed cells. The *YTHDF1* interacting RNA was obtained using RNA-immunoprecipitation assay, and the *SLC39A4* mRNA expression was analyzed using PCR-agarose gel electrophoresis. **K** Representative results of agarose gel electrophoresis. **L** The m⁶A-dependent regulation of *SLC39A4* by *YTHDF1* was examined using dual-luciferase reporter system carrying *SLC39A4* mutant-type (MUT) sequences and wild-type (WT) sequences. $N = 3$. *YTHDF1* YTH N⁶-methyladenosine RNA binding protein F1, *SLC39A4* Solute carrier family 39 member 4, GC gastric cancer, m⁶A N⁶-methyladenosine, EV empty vector, *YTHDF1*-OE *YTHDF1* overexpression plasmid, CDS coding sequence. The data is presented as the mean value \pm standard deviation, and $p < 0.05$ was considered statistically significant.

promoted cuproptosis resistance in colorectal cancer cells [41]. Therefore, *SLC39A4* may inhibit cuproptosis by modulating the PI3K/AKT signaling pathway. The Wnt signaling pathway, which promotes cancer, was also activated by *SLC39A4* [42]. The abnormal activation of the Wnt signaling pathway has been shown to confer resistance to cuproptosis in cancer stem cells [43]. The Wnt signaling pathway may mediate the inhibition of cuproptosis in cancer cells by *SLC39A4*. Based on existing reports, this study analyzed the phosphorylation processes in response to

SLC39A4 in GC cells using phosphorylation proteomics. The results of the kinase-substrate enrichment analysis indicate that the phosphorylation modifications induced by the overexpression of *SLC39A4* may be mediated by the kinase CSNK2A1. CSNK2A1 is an activator of the PI3K/AKT signaling pathway and promotes the progression of GC [44]. Based on previous studies, CSNK2A1-catalyzed phosphorylation may underlie the activation of the PI3K/AKT pathway by *SLC39A4*. This finding enhances our understanding of the detailed molecular mechanisms underlying the

signal cascade driven by SLC39A4. We found that overexpression of SLC39A4 increased the phosphorylation level of HSPB1. HSPB1 has been reported as a downstream target of activated p38, with phosphorylated p38 (p-p38) promoting the phosphorylation of HSPB1 at Ser82 [45, 46]. Therefore, it is possible that SLC39A4 induces HSPB1 phosphorylation through a mechanism involving p38 signaling pathway activation. Reports have shown that inhibition of the p38 signaling pathway leads to an enhancement of cuproptosis [47]. From the data obtained in this work, SLC39A4 may inhibit cuproptosis by activating the p38 signaling pathway.

The present study has quantified the influence of SLC39A4 and YTHDF1 on cuproptosis in GC cells. It has been reported that, similar to SLC39A4, YTHDF1 acts as an activator of the Wnt and PI3K/AKT signaling pathways [48, 49]. The abnormal activation of these pathways enhances cancer cell resistance to cuproptosis [41, 43]. Therefore, we can speculate that YTHDF1 promotes SLC39A4 translation by recognizing m6A modifications, thereby activating specific signaling pathways, such as the Wnt and PI3K/AKT pathways, and consequently inhibiting cuproptosis in GC cells.

CONCLUSION

Targeting SLC39A4 emerges as a crucial strategy for GC treatment. Elevated expression of SLC39A4, facilitated by the m6A reader YTHDF1 at the translational level, promotes GC progression by decreasing susceptibility to cuproptosis.

DATA AVAILABILITY

Data are available from the corresponding author on reasonable request.

REFERENCES

- Ramezankhani R, Solhi R, Es HA, Vosough M, Hassan M. Novel molecular targets in gastric adenocarcinoma. *Pharm Ther.* 2021;220:107714.
- Thrift AP, El-Serag HB. Burden of gastric cancer. *Clin Gastroenterol Hepatol.* 2020;18:534–42.
- Bray F, Laversanne M, Sung H, Ferlay J, Siegel RL, Soerjomataram I, et al. Global cancer statistics 2022: GLOBOCAN estimates of incidence and mortality worldwide for 36 cancers in 185 countries. *CA Cancer J Clin.* 2024;74:229–63.
- Smyth EC, Nilsson M, Grabsch HI, van Grieken NCT, Lordick F. Gastric cancer. *Lancet.* 2020;396:635–48.
- Xie J, Yang Y, Gao Y, He J. Cuproptosis: mechanisms and links with cancers. *Mol Cancer.* 2023;22:46.
- Tsvetkov P, Coy S, Petrova B, Dreishpoon M, Verma A, Abdusamad M, et al. Copper induces cell death by targeting lipoylated TCA cycle proteins. *Science.* 2022;375:1254–61.
- Sun L, Zhang Y, Yang B, Sun S, Zhang P, Luo Z, et al. Lactylation of METTL16 promotes cuproptosis via m(6)A-modification on FDX1 mRNA in gastric cancer. *Nat Commun.* 2023;14:6523.
- Zhang S, Huang Q, Ji T, Li Q, Hu C. Copper homeostasis and copper-induced cell death in tumor immunity: implications for therapeutic strategies in cancer immunotherapy. *Biomark Res.* 2024;12:130.
- Antala S, Dempski RE. The human ZIP4 transporter has two distinct binding affinities and mediates transport of multiple transition metals. *Biochemistry.* 2012;51:963–73.
- Weaver BP, Zhang Y, Hiscox S, Guo GL, Apte U, Taylor KM, et al. Zip4 (Slc39a4) expression is activated in hepatocellular carcinomas and functions to repress apoptosis, enhance cell cycle and increase migration. *PLoS One.* 2010;5:e13158.
- Ishida S, Kasamatsu A, Endo-Sakamoto Y, Nakashima D, Koide N, Takahara T, et al. Novel mechanism of aberrant ZIP4 expression with zinc supplementation in oral tumorigenesis. *Biochem Biophys Res Commun.* 2017;483:339–45.
- Liu M, Zhang Y, Yang J, Zhan H, Zhou Z, Jiang Y, et al. Zinc-dependent regulation of ZEB1 and YAP1 coactivation promotes epithelial-mesenchymal transition plasticity and metastasis in pancreatic cancer. *Gastroenterology.* 2021;160:1771–83. e1.
- Ding B, Lou W, Xu L, Li R, Fan W. Analysis the prognostic values of solute carrier (SLC) family 39 genes in gastric cancer. *Am J Transl Res.* 2019;11:486–98.
- Ren H, Liu C, Zhang C, Wu H, Zhang J, Wang Z, et al. A cuproptosis-related gene expression signature predicting clinical prognosis and immune responses in intrahepatic cholangiocarcinoma detected by single-cell RNA sequence analysis. *Cancer Cell Int.* 2024;24:92.
- Liu M, Zhang Y, Yang J, Cui X, Zhou Z, Zhan H, et al. ZIP4 increases expression of transcription factor ZEB1 to promote integrin α 3 β 1 signaling and inhibit expression of the gemcitabine transporter ENT1 in pancreatic cancer cells. *Gastroenterology.* 2020;158:679–92. e1.
- Shen M, Li K, Wang L, Feng L, Zhang X, Zhang H, et al. ZIP4 upregulation aggravates nucleus pulposus cell degradation by promoting inflammation and oxidative stress by mediating the HDAC4-FoxO3a axis. *Aging.* 2024;16:685–700.
- Zeng Q, Liu YM, Liu J, Han J, Guo JX, Lu S, et al. Inhibition of ZIP4 reverses epithelial-to-mesenchymal transition and enhances the radiosensitivity in human nasopharyngeal carcinoma cells. *Cell Death Dis.* 2019;10:588.
- Zhang Y, Bharadwaj U, Logsdon CD, Chen C, Yao Q, Li M. ZIP4 regulates pancreatic cancer cell growth by activating IL-6/STAT3 pathway through zinc finger transcription factor CREB. *Clin Cancer Res.* 2010;16:1423–30.
- You Q, Wang F, Du R, Pi J, Wang H, Huo Y, et al. m(6)A reader YTHDF1-targeting engineered small extracellular vesicles for gastric cancer therapy via epigenetic and immune regulation. *Adv Mater.* 2023;35:e2204910.
- Bai X, Wong CC, Pan Y, Chen H, Liu W, Zhai J, et al. Loss of YTHDF1 in gastric tumors restores sensitivity to antitumor immunity by recruiting mature dendritic cells. *J Immunother Cancer.* 2022;10:e003663.
- Liu T, Wei Q, Jin J, Luo Q, Liu Y, Yang Y, et al. The m6A reader YTHDF1 promotes ovarian cancer progression via augmenting EIF3C translation. *Nucleic Acids Res.* 2020;48:3816–31.
- Li Q, Ni Y, Zhang L, Jiang R, Xu J, Yang H, et al. HIF-1 α -induced expression of m6A reader YTHDF1 drives hypoxia-induced autophagy and malignancy of hepatocellular carcinoma by promoting ATG2A and ATG14 translation. *Signal Transduct Target Ther.* 2021;6:76.
- Zhang X, Su T, Wu Y, Cai Y, Wang L, Liang C, et al. N6-methyladenosine reader YTHDF1 promotes stemness and therapeutic resistance in hepatocellular carcinoma by enhancing NOTCH1 expression. *Cancer Res.* 2024;84:827–40.
- Wang Q, Chen C, Xu X, Shu C, Cao C, Wang Z, et al. APAF1-binding long non-coding RNA promotes tumor growth and multidrug resistance in gastric cancer by blocking apoptosome assembly. *Adv Sci.* 2022;9:e2201889.
- Necula L, Matei L, Dragu D, Pitica I, Neagu AI, Bleotu C, et al. High plasma levels of COL10A1 are associated with advanced tumor stage in gastric cancer patients. *World J Gastroenterol.* 2020;26:3024–33.
- Wang J, Ni Z, Duan Z, Wang G, Li F. Altered expression of hypoxia-inducible factor-1 α (HIF-1 α) and its regulatory genes in gastric cancer tissues. *PLoS One.* 2014;9:e99835.
- Li J-H, Liu S, Zhou H, Qu L-H, Yang J-H. starBase v2.0: decoding miRNA-ceRNA, miRNA-ncRNA and protein-RNA interaction networks from large-scale CLIP-Seq data. *Nucleic Acids Res.* 2014;42:D92–7.
- Fan R, Cui C, Kang B, Chang Z, Wang G, Cui Q. A combined deep learning framework for mammalian m6A site prediction. *Cell Genomics.* 2024;4:100697.
- Huang X-Y, Shen J-Y, Huang K, Wang L, Sethi G, Ma Z. Cuproptosis in cancers: function and implications from bench to bedside. *Biomed Pharmacother.* 2024;176:116874.
- Xia C, Chen X, Li J, Chen P. SLC39A4 as a novel prognosis marker promotes tumor progression in esophageal squamous cell carcinoma. *Onco Targets Ther.* 2020;13:3999–4008.
- Li M, Zhang Y, Liu Z, Bharadwaj U, Wang H, Wang X, et al. Aberrant expression of zinc transporter ZIP4 (SLC39A4) significantly contributes to human pancreatic cancer pathogenesis and progression. *Proc Natl Acad Sci USA.* 2007;104:18636–41.
- Pi J, Wang W, Ji M, Wang X, Wei X, Jin J, et al. YTHDF1 promotes gastric carcinogenesis by controlling translation of FZD7. *Cancer Res.* 2021;81:2651–65.
- Chen XY, Liang R, Yi YC, Fan HN, Chen M, Zhang J, et al. The m(6)A reader YTHDF1 facilitates the tumorigenesis and metastasis of gastric cancer via USP14 translation in an m(6)A-dependent manner. *Front Cell Dev Biol.* 2021;9:647702.
- Li Y, Guo X, Liang X, Wang Z. YTHDF1 promotes proliferation and inhibits apoptosis of gastric cancer cells via upregulating TCF7 mRNA translation. *Front Biosci.* 2024;29:117.
- Bai R, Sun M, Chen Y, Zhuo S, Song G, Wang T, et al. H19 recruited N6-methyladenosine (m6A) reader YTHDF1 to promote SCARB1 translation and facilitate angiogenesis in gastric cancer. *Chin Med J (Engl).* 2023;136:1719–31.
- Yang X, Liu QL, Xu W, Zhang YC, Yang Y, Ju LF, et al. m(6)A promotes R-loop formation to facilitate transcription termination. *Cell Res.* 2019;29:1035–8.
- Lee Y, Choe J, Park OH, Kim YK. Molecular mechanisms driving mRNA degradation by m(6)A modification. *Trends Genet.* 2020;36:177–88.
- Guo X, Li K, Jiang W, Hu Y, Xiao W, Huang Y, et al. RNA demethylase ALKBH5 prevents pancreatic cancer progression by posttranscriptional activation of PER1 in an m6A-YTHDF2-dependent manner. *Mol Cancer.* 2020;19:91.
- Zhang L, Wan Y, Zhang Z, Jiang Y, Gu Z, Ma X, et al. IGF2BP1 overexpression stabilizes PEG10 mRNA in an m6A-dependent manner and promotes endometrial cancer progression. *Theranostics.* 2021;11:1100–14.
- Li Y, Liu L. UKLF/PCBP2 axis governs the colorectal cancer development by transcriptionally activating SLC39A4. *Biochim Biophys Acta Mol Cell Res.* 2024;1871:119755.

41. Huang T, Zhang Y, Wu Y, Han X, Li L, Guo Z, et al. CEBPB dampens the cuproptosis sensitivity of colorectal cancer cells by facilitating the PI3K/AKT/mTOR signaling pathway. *Saudi J Gastroenterol.* 2024;30:381–8.
42. Guo H, Su R, Lu X, Zhang H, Wei X, Xu X. ZIP4 inhibits Ephrin-B1 ubiquitination, activating Wnt5A/JNK/ZEB1 to promote liver cancer metastasis. *Genes Dis.* 2024;11:101312.
43. Liu YT, Chen L, Li SJ, Wang WY, Wang YY, Yang QC, et al. Dysregulated Wnt/ β -catenin signaling confers resistance to cuproptosis in cancer cells. *Cell Death Differ.* 2024;31:1452–66.
44. Jiang C, Ma Z, Zhang G, Yang X, Du Q, Wang W. CSNK2A1 promotes gastric cancer invasion through the PI3K-Akt-mTOR signaling pathway. *Cancer Manag Res.* 2019;11:10135–43.
45. Sluzala ZB, Hamati A, Fort PE. Key role of phosphorylation in small heat shock protein regulation via oligomeric disaggregation and functional activation. *Cells.* 2025;14:127.
46. Tao Y, Wang H, Peng Y, Chen Y, Liu X, Qi G, et al. Ceramide kinase suppresses ferroptosis and protects against alcohol-associated liver disease through the p38 MAPK-HSPB1 pathway. *HepatoL Commun.* 2025;9:e0731.
47. Wang X, Jia JH, Zhang M, Meng QS, Yan BW, Ma ZY, et al. Adrenomedullin/FOXO3 enhances sunitinib resistance in clear cell renal cell carcinoma by inhibiting FDX1 expression and cuproptosis. *FASEB J.* 2023;37:e23143.
48. Yang X, Lin Y, Chen T, Hu W, Li P, Qiu X, et al. YTHDF1 enhances chondrogenic differentiation by activating the Wnt/ β -catenin signaling pathway. *Stem Cells Dev.* 2023;32:115–30.
49. Luo X, Cao M, Gao F, He X. YTHDF1 promotes hepatocellular carcinoma progression via activating PI3K/AKT/mTOR signaling pathway and inducing epithelial-mesenchymal transition. *Exp Hematol Oncol.* 2021;10:35.

ACKNOWLEDGEMENTS

This study was funded by a grant from the Xinjiang Production and Construction Corps (No. 2023AB018-01). Importantly, the funders did not participate in the study's design, data collection and analysis, decision to publish, or manuscript preparation.

AUTHOR CONTRIBUTIONS

J.Y.S. & J.H.Q.: conceptualization, methodology, data curation, writing – original draft. B.H.X. & J.X.W.: methodology, investigation, data curation. Ram Prasad Chaulagain & H.L.C.: investigation, formal analysis, data curation. N.L. & X.Y.J.: validation, formal analysis, data curation. L.Y.X., F.C.L. & W.L.M.: validation, software, visualization, data curation. S.Z.J., resources, funding acquisition, supervision, writing – review & editing.

FUNDING

This study was funded by a grant from the Xinjiang Production and Construction Corps (No. 2023AB018-01).

COMPETING INTERESTS

The authors declare no competing interests.

ETHICAL APPROVAL

All clinical experimental procedures received approval from the Ethics Committee of the Second Affiliated Hospital of Harbin Medical University (No. YJSKY2024-376) and strictly adhered to the Declaration of Helsinki. The animal experiments were approved by the Ethics Committee of the Second Affiliated Hospital of Harbin Medical University (No. YJSDW2024-189).

ADDITIONAL INFORMATION

Supplementary information The online version contains supplementary material available at <https://doi.org/10.1038/s41417-026-01036-5>.

Correspondence and requests for materials should be addressed to Shizhu Jin.

Reprints and permission information is available at <http://www.nature.com/reprints>

Publisher's note Springer Nature remains neutral with regard to jurisdictional claims in published maps and institutional affiliations.



Open Access This article is licensed under a Creative Commons Attribution-NonCommercial-NoDerivatives 4.0 International License, which permits any non-commercial use, sharing, distribution and reproduction in any medium or format, as long as you give appropriate credit to the original author(s) and the source, provide a link to the Creative Commons licence, and indicate if you modified the licensed material. You do not have permission under this licence to share adapted material derived from this article or parts of it. The images or other third party material in this article are included in the article's Creative Commons licence, unless indicated otherwise in a credit line to the material. If material is not included in the article's Creative Commons licence and your intended use is not permitted by statutory regulation or exceeds the permitted use, you will need to obtain permission directly from the copyright holder. To view a copy of this licence, visit <http://creativecommons.org/licenses/by-nc-nd/4.0/>.

© The Author(s) 2026